Available online at www.sciencedirect.com
ScienceDirect
Journal of Petroleum Science and Engineering 54 (2006) 93–111
JOURNAL OF PETROLEUM SCIENCE & ENGINEERING
www.elsevier.com/locate/petrol

# Wormhole initiation and propagation of emulsified acid in carbonate cores using computerized tomography

Shameem Siddiqui *, Hisham A. Nasr-El-Din, Aon A. Khamees

*Saudi Aramco, Box 62, Dhahran 31311, Saudi Arabia*

Received 20 December 2005; received in revised form 24 July 2006; accepted 2 August 2006

**Abstract**

Emulsified acids are widely used for stimulating carbonate reservoirs. This study examines alternate ways to evaluate the performance of emulsified acids by using a non-destructive visual-based technique. Using advanced image processing software and techniques, it was possible to examine the dissolution patterns created by emulsified acids at different operating conditions. Computerized Tomography (CT) was successful in monitoring wormhole initiation and growth inside carbonate core plugs during the injection of emulsified acid.

The emulsified acid systems used were successful in creating a barrier for the acid allowing its slow release away from the injection face. The reaction appeared to take place simultaneously at different places inside the core resulting in channels, which later joined together to form a continuous wormhole between the inlet and outlet ends of the core plug.

The presence of natural channels (vugs, stylolites, etc.) and higher concentrations of calcite may help faster wormhole initiation. Injection rate appeared to be the most important factor affecting emulsified acid performance in terms of wormhole initiation and growth (faster injection caused faster wormhole initiation and consequently, its growth). Animations based on CT-scanner generated data and created using advanced three-dimensional (3-D) image processing packages proved to be extremely useful in observing the changes taking place inside the cores during emulsified acid injection. The methodology developed for conducting the test and evaluating the image data can be applied to other tests involving visual-based evaluation of laboratory treatments.
© 2006 Elsevier B.V. All rights reserved.

*Keywords:* Matrix acidizing; Emulsified acid; Wormholes; Computerized tomography

## 1. Introduction

Hydrochloric acid (HCl) is commonly used to stimulate carbonate reservoirs. This acid reacts very rapidly with calcite. Therefore, there is a need to retard acid reaction so that a deep acid penetration can be achieved. This goal can be achieved using emulsified acid. The acid can be emulsified using a hydrocarbon phase (diesel or xylene) and a suitable emulsifier. Emulsified acids present a definite advantage over ordinary acids as the hydrocarbon phase provides a diffusion barrier causing the slow release of acid and deeper penetration.

The evaluation of the performance of emulsified acids is generally based on the comparison of the

* Corresponding author. Now at Texas Tech University, PE Department, Lubbock, TX, USA. Fax: +1 806 742 3502.
*E-mail addresses:* shameem.siddiqui@ttu.edu (S. Siddiqui), hisham.nasreldin@aramco.com (H.A. Nasr-El-Din), aon.khamees@aramco.com (A.A. Khamees).

0920-4105/$ - see front matter © 2006 Elsevier B.V. All rights reserved.
doi:10.1016/j.petrol.2006.08.005

pressure drops across the core before and after the acid treatment. The ratio of the two pressure drops, with all other parameters being constant, gives the $k/k_0$ ratio or the permeability improvement. However, this analysis does not give any information about the initiation and growth rate of the wormholes created by the acid. This study examines the use of a visual technique based on CT-scanning for evaluating emulsified acid performance.

A methodology was developed for collecting emulsified acid injection data on the core plugs through the non-destructive use of CT and then to use image processing packages to view the changes. The objectives of this study are: (1) to conduct coreflooding experiments with an emulsified acid system for a particular set of operating conditions while investigating the changes in reservoir cores with the CT, and (2) to evaluate the performance of this acid system using the image subtraction technique.

## 2. Background

### 2.1. Computerized tomography

CT has been used extensively by the petroleum industry for the last two decades for studying reservoir rocks and rock-fluid systems in a non-destructive manner. The use of CT-scanning in the petroleum industry covers two major areas: core characterization and fluid flow visualization in porous media. For the former, the rock samples are mostly scanned in as-received conditions, but for the latter, almost always fluids containing a radiopaque tracer are used to enhance the CT attenuations. Reviews of the various applications of CT in the petroleum industry can be found in the literature (Vinegar, 1986; Vinegar and Wellington, 1987; Wellington and Vinegar, 1987; Hunt et al., 1988; Withjack, 1988; Kantzas, 1990; Akin and Kovscek, 2001; Withjack et al., 2003).

Until recently, almost all the petroleum industry applications of CT utilized modified medical CT-scanners. The medical CT attenuation data are presented in an internationally standardized attenuation scale called the Hounsfield unit. The unit is based on the CT number (CTN) of air at −1000 and the CTN for water at 0 Hounsfield units. The attenuation measured by a CT-scanner is a function of both the bulk density ($\rho_b$) and effective atomic number ($Z_{eff}$) of the object scanned. The dual-energy based method involves scanning the core twice at the same location, using a high- and a low-energy setting. For reservoir cores, the dual-energy derived $Z_{eff,}$ and $\rho_b$ data can potentially yield the mineralogy of the core plugs (Wellington and Vinegar, 1987; Siddiqui and Khamees, 2004).

### 2.2. Matrix acidizing and wormholes

Matrix acidizing of oil reservoirs is a process designed to improve well productivity by increasing rock permeability in the region surrounding the wellbore (Hoefner and Fogler, 1985). Acid stimulation of production and injection wells is routinely used to remove pore plugging deposits from damaged wells. These types of plugging are detrimental when they occur in the immediate vicinity of the wellbore where they form a low-permeability skin. This near wellbore permeability reduction can be effectively removed by proper acid treatments. Matrix acidizing can also enhance production in wells that exhibit low natural formation permeability. In this case permeability increase is achieved by partial dissolution of the original rock matrix instead of by removal of particulates. Natural flow channels are enlarged allowing increased production.

The high reaction rate of HCl with calcite results in the formation of large flow channels called wormholes. Wormholes are created because of the high dissolution rates that are encountered in carbonate formations. Wormholes originate at the wellbore and extend radially in random direction into the formation. Wormholes form because of the heterogeneity of natural porous media and the non-uniform flow or channeling that always results. Some areas of the rock receive more flow than others. Acid penetrates farther into those regions and so dissolution is accelerated there. Local permeability is increased through enlargement of pores and pore throats and flow increases even more. A dominant channel quickly forms which then grows in length and propagates through the medium. Once wormholes form they carry essentially most of the fluid and regions near the wellbore, but not near the wormhole experience virtually no flow because of the negligible resistance to flow in the wormhole itself (Hoefner and Fogler, 1985). According to Williams et al. (1979) neither theoretical nor experimental studies can predict the number, size, or length of wormholes. If acid reaction rate is very fast, the theories predict that only a few wormholes will form. A slow reaction rate favors the formation of several small-diameter wormholes. Nierode and Williams (1971) showed that the maximum wormhole length ranges from a few inches to a few feet and its length can be substantially increased by reducing the rate of fluid loss from the wormhole to the formation.

Hydrochloric acid containing a fluid-loss additive is effective in controlling the rate of fluid loss to the formation during acidizing. In low-permeability formations, it is not feasible to use these acids because of their

low injectivity and using of up to 28 wt.% HCl is normally preferred (Williams et al., 1979). If HCl cannot be sufficiently inhibited to reduce corrosion at the formation temperature, formic acid is preferred although acetic acid can also be used.

At present, there is no established method to evaluate the initiation and growth of wormhole inside rocks. A destructive approach for evaluating wormholes inside acid-treated core plugs involves forcing Wood's metal through the wormhole created and then dissolving the carbonate matrix with an acid to examine the shape of the wormhole retained by the Wood's metal. However, the use of a CT-scanner in conjunction with a laboratory acidizing setup is most effective. Not only does it allow the evaluation of the wormholes after acidizing, but it also allows viewing all the changes taking place inside the core plug in a non-destructive manner. Bazin et al. (1995) and Bazin and Abdulahad (1999) used subtraction of CT-scan images before and after acidizing for the three-dimensional reconstruction of wormholes created. There is no published data dealing with wormhole initiation and growth for the case of emulsified acids, which is a unique feature of the present study.

### 2.3. Emulsified acid

In carbonate reservoirs, the reaction rate of hydrochloric acid with calcite is very fast (Nierode and Williams, 1971). In conventional stimulations where 15 wt.% HCl is used at low flow rates, the acid reacts with the carbonate rock and causes surface wash-out only (Hoefner et al., 1987). This means that the acid will not penetrate the damaged zone and, as a result, the efficiency of the stimulation treatment will be low. One way to overcome this problem is to use acid-in-diesel emulsions. Diesel acts as a diffusion barrier between the acid and the rock (Hoefner and Fogler, 1985). Thus, the reaction rate of the acid with carbonate rocks becomes slower. This gives the acid the ability to penetrate deeper into the formation by creating wormholes, which enhance well performance.

Acid-in-diesel emulsion has several advantages besides its slow reaction rate with the rock. First, it has a relatively high viscosity. As a result, it has better sweep efficiency that will improve acid distribution in heterogeneous reservoirs (Buijse, 2000). The live acid has minimum contact with the well tubulars. Therefore, there is minimum corrosion to well casing and tubing. As a result, the concentration of total iron in the live acid reaching the formation is low (Al-Anazi et al., 1998). This will minimize the amount of iron control agents needed to prevent iron precipitation and other problems that created by the presence of iron ions, especially ferric iron.

Emulsified acid has been successfully used to stimulate oil wells, water disposal wells, tight gas wells in Saudi Arabia and elsewhere (Al-Anazi et al., 1998; Mohamed et al., 1999; Navarrete et al., 2000; Nasr-El-Din et al., 2000; Bartko et al., 2003). The desirable properties of emulsified acids are the same as for straight acids – formation of long wormholes. The structure of the wormholes depends on the competition between the convective transport of acid (injection rate) and the acid reaction rate with the rock (Navarrete et al., 2000). Typical structures range from face dissolution at low injection rates and/or high reaction rates (complete dissolution of the rock starting radially from the wellbore) to ramified wormhole structures at high injection rates and/or low injection rates. Single dominant wormholes are formed at intermediate injection rates. Face dissolution does not result in significant skin reduction; instead long single wormholes maximize skin reduction (Navarrete et al., 2000). The high viscosity of emulsified acids is useful in matrix applications to improve the distribution of acid in different permeability zones. High-temperature stability is another desirable property of the emulsified acid.

Bazin and Abdulahad (1999) conducted a large number of coreflooding experiments with different emulsified acid systems. Limestone cores of 2-in. diameter × 8-in. long cores (permeability varying from 1.5 to 3.3 mD) were used. Their tests also included emulsion stability and measuring the apparent viscosity of different acid-in-diesel emulsions. The emulsifiers examined included a petroleum sulfonate surfactant (Witco Petronate HH, which requires an alcohol to be added) and a nonionic emulsifier IPE101 (IFP product, which requires no alcohol, but was used at a higher surfactant concentration). They also studied the dissolution patterns using CT. Their findings were as follows:

- Increasing the diesel volume fraction in the emulsified acid system increases emulsion stability and the apparent viscosity of the emulsion. A system with 50/50 diesel/acid volume ratio has acceptable properties.
- The effect of emulsifier type on the performance of emulsified acid was not significant.
- Increasing the acid concentration provides higher penetration rates,
- Increasing the acid volume in the emulsion formulation does not decrease the acid breakthrough time significantly.
- Numerous tests confirmed the existence of an optimum injection rate (a lowest value in the

wormhole breakthrough time versus injection rate plot) for regular acid systems. This optimum rate is a direct function of the core length and is related to acid consumption and maximum wormhole penetration. For the acid-in-oil emulsions tested, no such optimum rate was observed in the range of flow rates investigated in their experimental study.

The dissolution patterns (wormholes) obtained using X-ray radiographs were very thin and nearly invisible at all the flow rates tested, these contrasted with those formed using straight acids. CT image subtraction based data for both of the emulsified acid systems tested (Petronate and IP) showed uniform dissolution, with numerous channels. These thin dissolution channels may actually improve the permeability slightly.

Navarrete et al. (2000) developed emulsified acid systems that were stable up to 350 °F. Their emulsified acid system produced higher fracture conductivities than straight acids and was 14 to 19 times more retarded than the latter at temperatures between 250 and 350 °F. Hoefner and Fogler (1985) developed a micro-emulsion based system using dodecane, water (aqueous HCl), cetylpyridinium chloride and butanol as co-surfactant. They added a cationic surfactant for increased micro-emulsion stability at higher temperatures. Their system was tested on very homogeneous, but low-permeability Danian chalks, which are almost impossible to stimulate with straight acid and it was quite effective. The fluid penetrated much farther into limestone matrix before acid could diffuse to the pore wall and react. The tests also required only a fraction of the total volume of injected fluid compared to straight HCl.

The main objective of the present study is to examine initiation and propagation of wormhole generated by emulsified acid in carbonate cores. The effects of core initial permeability and acid injection rate on wormhole propagation were also examined.

### 2.4. Experimental studies

The procedure used to conduct coreflood experiments was as follows:

- Select a carbonate core plug.
- Prepare the emulsified acid and the brine (doped with 10 wt.% NaI).
- Put the core plug inside a special coreholder (X-ray transparent).
- Apply a confining pressure that matches the reservoir overburden (3,000 psi (20.7 MPa)).
- Vacuum-saturate the core plug with the doped brine.
- Inject the emulsified acid into the carbonate core plugs.
- Displace the acid out of the system with the doped brine.

During the coreflood experiments, the coreholder was scanned at the same locations using a CT-scanner to obtain a series of images of the plug undergoing the acid treatment. The primary equipment used was an HD-350 CT-scanner with a maximum voltage rating of 140 kV and a maximum intensity of 200 mA. The specially designed experimental set-up (Fig. 1) allowed conducting tests with visualization of the simultaneous motions of various fluids inside cores. The experimental set-up consisted of a special low X-ray attenuation core holder, a four-cylinder positive displacement pump, a vacuum pump, a balance, two floating piston accumulators, stainless steel valves, and polyetheretherketone (PEEK) and stainless steel tubing.

### 2.5. Core data and test procedure

Tests were conducted using emulsified acid on three low-permeability core plug samples from a well in an Upper Jurassic oil reservoir in Saudi Arabia. They were all vertical plugs and referred to as Samples U1V, U2V and U3V, respectively. All of these samples were acidized with 20 wt.% HCl emulsified acid. The acid contained 0.2 vol.% corrosion inhibitor, while the diesel phase contained 1 vol.% emulsifier. The acid to diesel volume ratio was 70:30. Only the acid injection rate and the rock samples were varied in these tests. The properties of core plugs and fluids are given in Table 1.

The apparent viscosity of the emulsified acid was measured as a function of shear rate using a Brookfield viscometer. Fig. 2 shows that the apparent viscosity of the emulsion decreased with the shear rate, highlighting the shear thinning behavior of this acid. In addition, the mean droplet size was measured using a laser particle analyzer. The mean droplet size of the acid droplets was found to be nearly 5 μm.

The procedure was the same for all tests, which included the following steps:

- Put the plug in a low X-ray attenuation coreholder and apply 3,000 psi (20.7 MPa) confining pressure,
- Pull vacuum from the outlet end of the core for several hours. Then, scan the core plug at two energies: high at 140 kV, 100 mA; and low at 80 kV, 200 mA, both with 5-mm beam thickness and 5 mm slice interval at fixed scan locations.
- Saturate the core with brine tagged with 10 wt.% NaI.

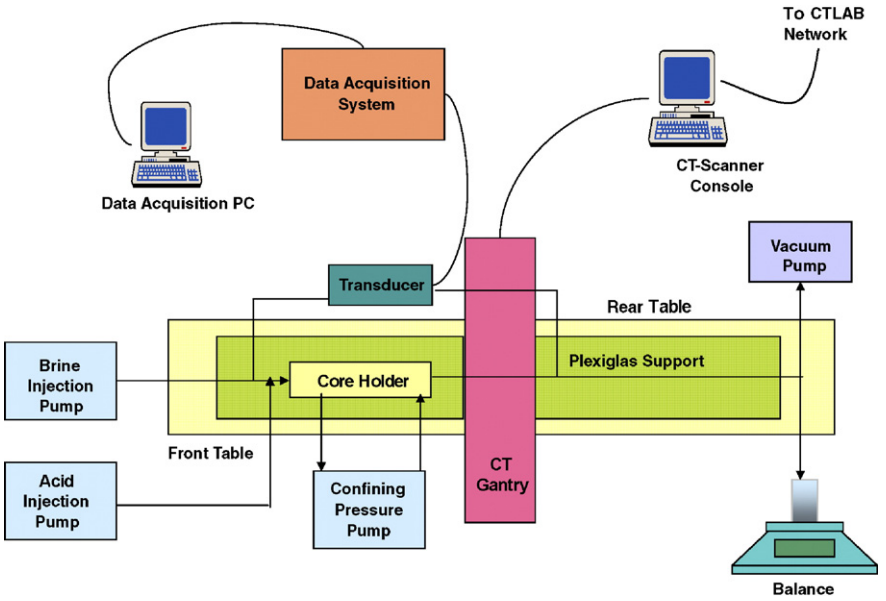


Fig. 1. A schematic diagram of the experimental setup.

- With no appreciable fluid intake, switch to the pumps and flow at least five pore volumes (PV) of brine to make sure that the core is fully saturated. Use three different rates (if possible) and record corresponding pressures for initial permeability measurement.
- Scan the core at the high energy setting at the same locations mentioned above, to obtain the wet scan images.
- Connect the floating piston accumulator containing freshly-made emulsified acid solution to the pump outlet and flow through by-pass to clean the lines.

Table 1
Characteristics of core samples U1V, U2V, U3V and fluid properties

| Core and fluid data | U1V before the test | U1V after the test | U2V before the test | U2V after the test | U3V before the test | U3V after the test |
|---|---|---|---|---|---|---|
| Weight (g) | 135.93 | 134.72 | 146.29 | 145.24 | 104.71 | 103.7 |
| Length (cm) | 1.97 | 1.97 | 2.11 | 2.11 | 1.49 | 1.49 |
| Diameter (cm) | 1.49 | 1.49 | 1.49 | 1.49 | 1.49 | 1.49 |
| Grain volume ($cm^3$) | 50.56 | 49.76 | 54.36 | 53.76 | 39.01 | 38.45 |
| Grain density ($g/cm^3$) | 2.69 | 2.71 | 2.69 | 2.70 | 2.68 | 2.70 |
| Bulk volume ($cm^3$) | 56.29 | 56.29 | 60.29 | 60.29 | 42.57 | 42.57 |
| Pore volume ($cm^3$) | 5.73 | 6.53 | 5.93 | 6.53 | 3.57 | 4.13 |
| Bulk density ($g/cm^3$) | 2.41 | 2.39 | 2.43 | 2.41 | 2.46 | 2.44 |
| Porosity (vol.%) | 10.18% | 11.60% | 9.83% | 10.83% | 8.38 | 9.70 |
| Air permeability (mD) [a] | 0.27 | 3,202.8 | 0.13 | 6,940.1 | 0.17 | 2,580.7 |
| Brine permeability [b] (mD) | 0.06 | 27.5 | 0.08 | 117.8 | 0.04 | 27.7 |
| Brine phase [c] | 10 wt.% NaI | | 10 wt.% NaI | | 10 wt.% NaI | |
| Brine density [d] ($g/cm^3$) | 1.080 | | 1.080 | | 1.080 | |
| Brine viscosity [d] (cp) | 1.009 | | 1.009 | | 1.009 | |
| Acid phase | 20 wt.% HCl | | 20 wt.% HCl | | 20 wtd% HCl | |
| Acid injection rate ($cm^3$/min) | 1.0 | | 0.2 | | 0.5 | |

[a] Air permeability was measured at 200 (1.38 MPa) psi confining pressure.
[b] Brine permeability was measured at 3,000 psi (20.7 MPa) confining pressure.
[c] Brine phase was prepared using distilled water.
[d] Density and viscosity were measured at ambient conditions.

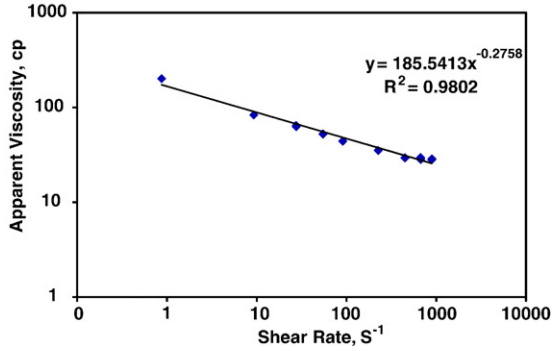


Fig. 2. Apparent viscosity versus shear rate for the emulsified acid system used.

- Start injecting the acid and take scans continuously while the acid is being pumped. Scan at least 10 cycles to generate enough three-dimensional CT-data for future visualization and evaluation purposes.
- After injecting the required volume of acid, stop the acid flow, then take a final scan.
- Connect the brine cylinder and pump brine into the core to remove as much acid as possible.
- Inject brine at the same three rates and record corresponding pump cylinder pressures for post-acidizing permeability measurement.
- Scan the core at the end of the brine injection, dry the core by flowing air and dismantle the coreholder to take the core out for drying for post-acidizing conventional core analysis measurements.
- Clean all connecting lines and the coreholder thoroughly with water to remove residual acid from the system.

It should be mentioned that the above procedure was adopted after several tests were made to optimize the process. Usually any coreflooding test involving a CT-scanner requires one of the fluids to be tagged with a radiopaque material (to increase attenuation of that phase) such as sodium iodide (NaI) in the aqueous phase) or iodo-dodecane ($C_{12}H_{25}I$) in the diesel phase of the emulsified acid. The former was chosen because it allowed better visualization for the conditions of the test.

## 3. Results from the high flow rate case using core U1V

### 3.1. CT-scanning sequences and images

A dual-energy based mineral characterization revealed the Sample U1V to be rich in calcite. The procedure, described by Siddiqui and Khamees (2004), involves scanning the core at the same locations twice, once with a high-energy setting to take advantage of the Compton Scattering Effect and then with a low-energy setting to take advantage of the Photoelectric Effect. The dual-energy CT-derived grain density (with the assumption that only calcite and dolomite are present in the core) was found to be 2.73 g/cm$^3$ (slightly higher than the conventional core analysis derived values of 2.69 g/cm$^3$ prior to test). Dual-energy data were also used to find the locations within the core that have high concentration of calcite, which is discussed later in this paper.

A total of 19 stages (or sequences) of CT image data were collected on Sample U1V during the test. In each scan sequence, the core was scanned at 9 positions (marked from 0 through 8 in the slice images), 5-mm apart from each other. The time taken between two subsequent slices was 8 s on the average (includes both scanning and reconstruction times) and the average time difference between the first and the ninth slices in a sequence was 72 s. At the flow rate of acid used (1 cm$^3$/min), this represents a difference of 1.2 cm$^3$ or 0.184 PVI (Pore Volumes Injected). The important sequences are given in Table 2.

After pulling vacuum, scanning at two energies, saturating using vacuum and flowing through it for permeability measurement, the core was scanned in fully brine saturated conditions to generate image data for the baseline (Sequence F). The brine pump valve was closed and the acid pump was connected to the core. A pressure of 1500 psi (10.3 MPa) was built prior to opening the valve for acid to the core. Injection of acid at 1 cm$^3$/min began and 1 min later the core was scanned in Sequence G. Acidizing was continued until Sequence N.

Fig. 3a (Sequence G) shows that it took a very short time for the acid to start making changes to the core. It took 74 s to begin the scanning of the first slice (0.19 PVI) in Sequence G. By the time the last scan was completed (72 s later, i.e., 0.37 PVI), acid was already seen developing significant wormholes (white spots), especially in the last three slices. By taking the position of the acid in the fifth slice (20 mm from first scanning position)

Table 2
CT-scanning sequences for plug U1V (1 cm$^3$/min)

| Sequence name | Description | PVI acid at the start |
|---|---|---|
| F | Scan of the brine saturated core | 0.00 |
| G | Start acid injection. at 1 cm$^3$/min | 0.19 |
| H | Continue acid injection | 0.61 |
| I | Continue acid injection | 0.95 |
| J | Continue acid injection | 1.29 |
| K | Continue acid injection | 1.59 |
| L | Continue acid injection | 1.92 |
| M | Continue acid injection | 2.47 |
| N | End of acid injection | 3.25 |

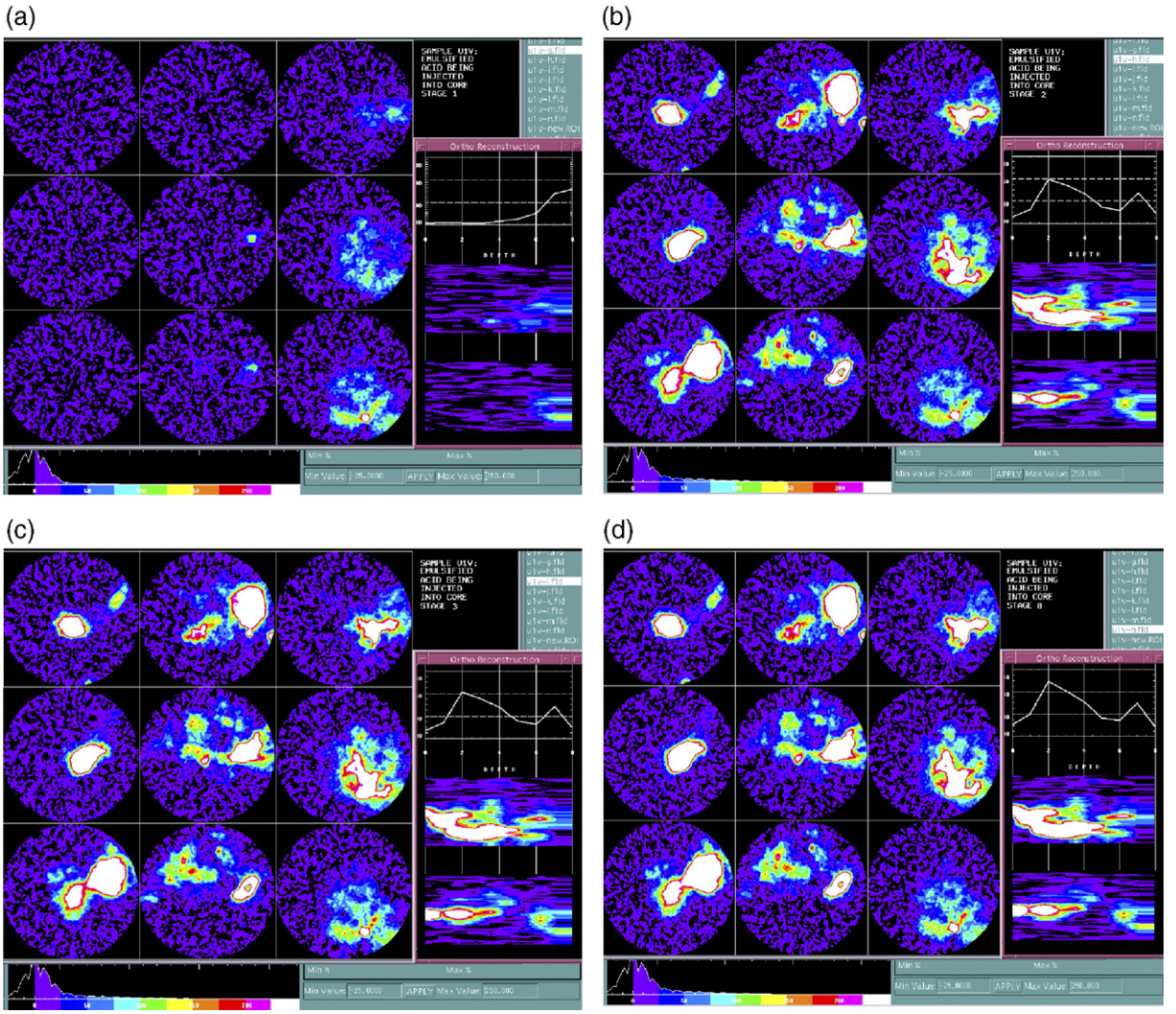


Fig. 3. a, b, c and d: Four image plates showing the core plug undergoing acid injection. Beginning of acid injection (Sequence G, Fig. 3(a)); the wormhole is fully developed (Sequence H, Fig. 3(b); and results of more acid injection (Sequences I and N; Fig. 3(c) and 3(d)). After the sequence N, acid injection was stopped.

as the beginning of wormhole there, it took 1 min–46 s (0.271 PVI) for the acid to reach the fifth slice. Three slice images in Fig. 3(a) may indicate a delay effect (acid passing through part of the plug before actual wormhole development), which may be caused by the slow release of the acid from the emulsified acid. This is discussed in more detail later in the paper. Fig. 3(b) and (c), which represent Sequences H and I (0.61 and 0.95 PVI, respectively), show continuation of the wormhole creation process by acid, the path of which appears to be complete. Fig. 3(d), which represents the last sequence before acid injection is stopped (3.25 PVI), shows very slight changes in slice colors compared to the previous sequences. This is because acid flowed easily through the path already created, without apparently making the wormhole any larger. After the scanning of Sequence N, the brine was flowed through the core to flush out the acid and conduct post-acid permeability measurements.

Several three-dimensional mpeg (Moving Pictures Expert Group) animations (movies) based on Sequences G through N during the emulsified acid injection were generated. For the movies three-dimensional data ($220 \times 220 \times 9$ data matrix) from all the sequences (G through N) were loaded simultaneously into an image processing program and animations were created by running through each sequence. Fig. 4 shows several snapshots from one such animation file. Only four out of the nine slices representing the entire core plug are shown to avoid cluttering of the display area. The injection end of the core plug is on the left and the

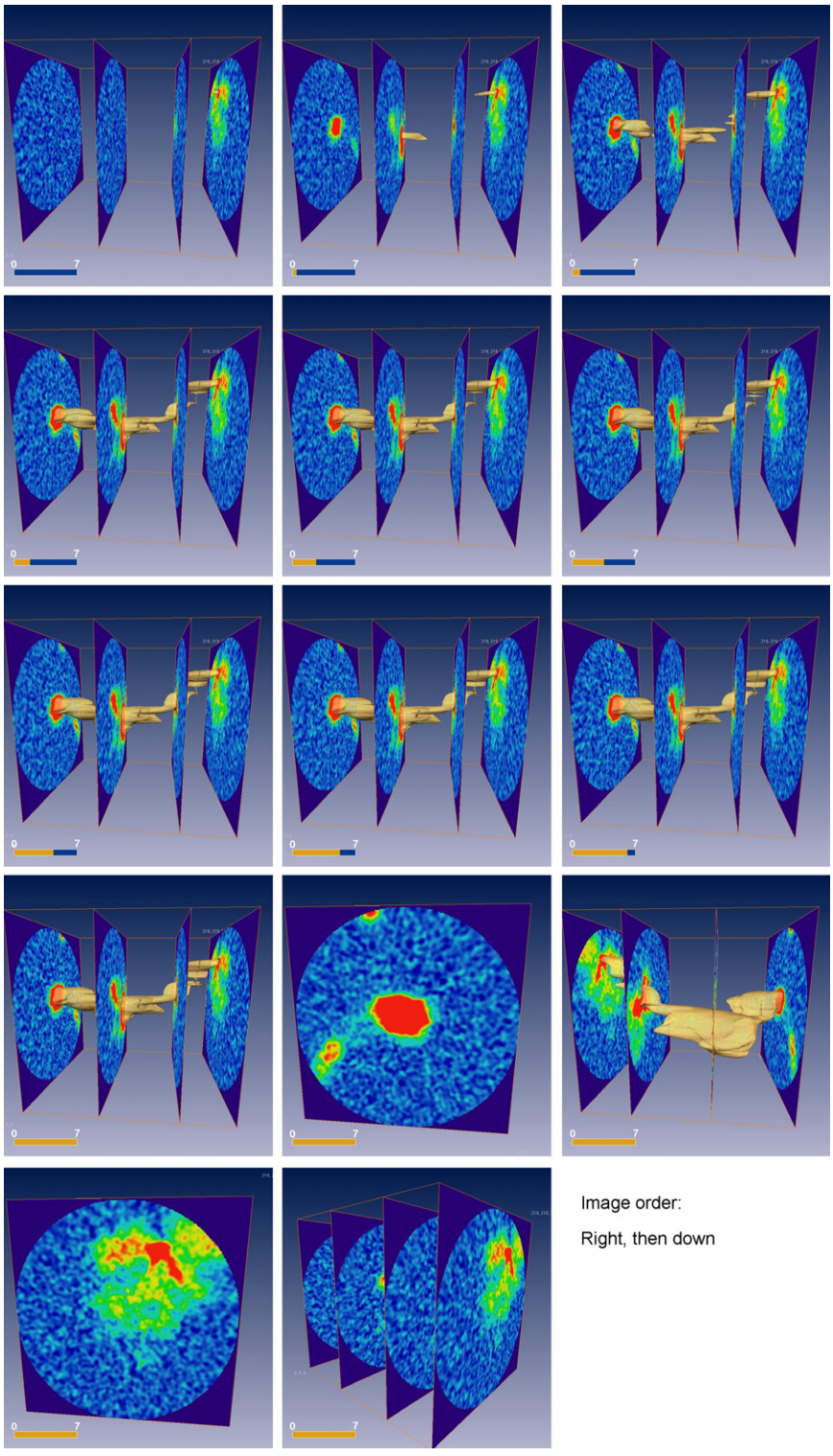


Fig. 4. Snapshots from a three-dimensional movie for the plug U1V showing the changes taking place inside the core during acidizing. The core is rotated at the last four snapshots to show the two ends.

production end is on the right. The wormhole is shown by a constantly-growing isosurface.

### 3.2. Summary of high flow rate case using core U1V

This test involving sample U1V, especially with the aid of the three-dimensional movies, allowed several observations to be made on emulsified acid performance. These findings are given below.

- The injection of emulsified acid was not an immiscible displacement i.e., acid pushing the brine as a front ahead of it, similar to the drainage process, shown in Fig. 5, which was seen inside three-plug composite core from the same Upper Jurassic reservoir during a CT-assisted coreflooding test (Siddiqui et al., 2000).
- The initiating of the wormhole with the emulsified acid is an in-situ process. Once the already injected acid reacts with sufficient amount of rock, an elongated channel is created (can be anywhere and not necessarily initiating at the core inlet), the subsequent acid displacement then connects the different channels to form a continuous wormhole.
- At the rate of injection used (1 $cm^3$/min) the reaction was very fast and the wormhole started being seen in the CT slices from around 0.37 PVI.
- The wormhole initiation and growth in Sample U1V seemed to be influenced by a higher concentration of calcite as can be seen in Fig. 6.
- For the test involving Sample U1V and 1 $cm^3$/min rate, the wormhole growth appeared to have initiated at the outlet end of the core (right) rather than at the inlet side. The resolution and detectability limit of the CT-scanner may be partly responsible for this appearance even though the initiation of the wormhole may actually have been near the inlet end. Using the same CT-scanner, Siddiqui et al. (2005) found the detectability limit for the cuttings to be about 2.4 mm (resolution of the scanner being about 0.46 mm) so it is possible for the scanner to miss the wormhole at the time of its entry.
- Although the lag due to CT-data acquisition and reconstruction (amounts to 72 s between the first and the last slice in this case) may partly obscure what was happening in the prior slices at the time when the last three slices were scanned in Sequence G, it appeared from the movie that the detectable wormhole did initiate at the outlet side of the plug. This apparent delay (acid transporting without reacting at the inlet end first) may actually have been caused by acid being present as a dispersed phase in diesel. This means that this acid is retarded and, as a result, will penetrate deeper into the formation. Tests on longer cores with faster CT-scanners may provide more insights into the subject.

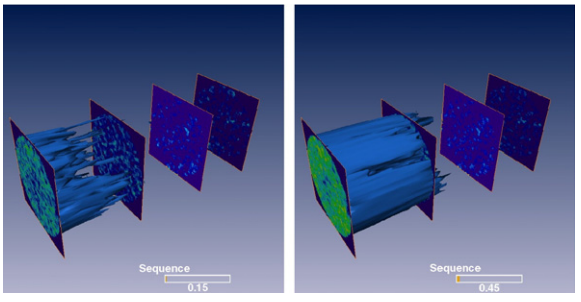


Fig. 5. Two snapshots from a movie showing oil (gray) displacing water (transparent) inside a composite core from a well in the same Upper Jurassic oil reservoir during the drainage phase of a coreflooding test. This immiscible displacement (injection from the left corner) is almost piston-like.

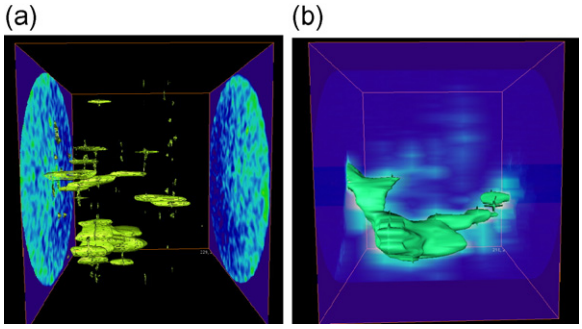


Fig. 6. (a) and (b): Dual-energy derived effective atomic number data showing locations inside the core plug U1V where calcite concentration is the highest (Fig. 6(a)). Post-acidizing data showing the wormhole location inside the core plug (Fig. 6(b)).

Table 3
CT-scanning sequences for plug U2V (0.2 $cm^3$/min)

| Sequence name | Description | PVI acid at the start |
|---|---|---|
| D | Scan of saturated core | 0.00 |
| E | First sequence after acid injection started | 0.04 |
| F | Continue acid injection | 0.11 |
| G | Continue acid injection | 0.18 |
| H | Continue acid injection | 0.25 |
| I | Continue acid injection | 0.32 |
| J | Continue acid injection | 0.39 |
| K | Continue acid injection | 0.47 |
| L | Continue acid injection | 0.54 |
| M | Continue acid injection | 0.62 |
| N | Continue acid injection | 0.70 |
| O | Continue acid injection | 1.40 |
| P | End injection at 0.2 $cm^3$/min | 2.02 |
| Q | End acid injection at 1 $cm^3$/min | 3.66 |
| R | End acid injection at 5 $cm^3$/min | 7.13 |

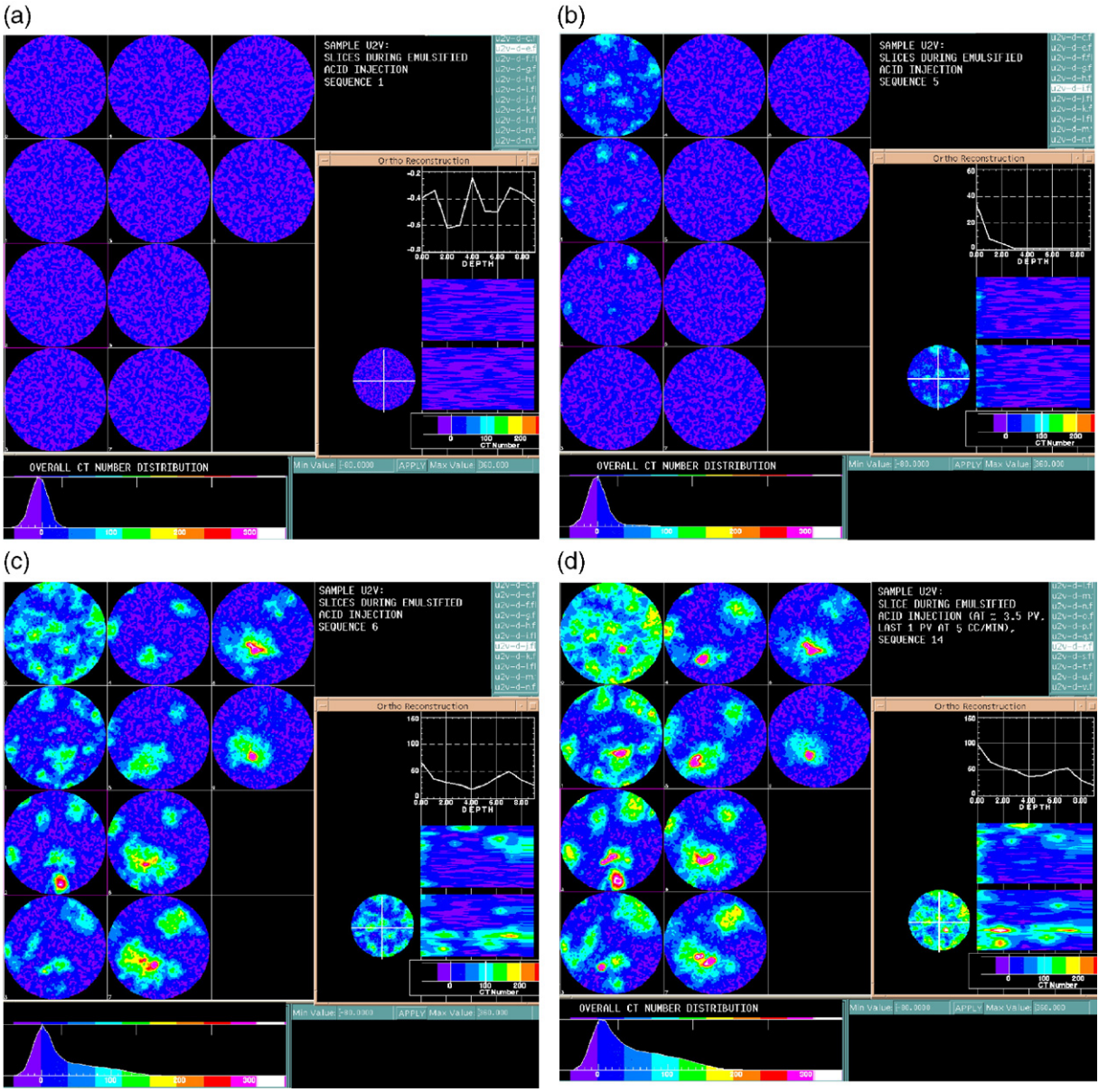


Fig. 7. (a) through (d): Slice images of the core plug U2V right after the acid injection was started (Sequence E, Fig. 7(a)). The wormhole is starting to develop (Sequence I, Fig. 7(b)). The wormhole is fully developed (Sequence J, Fig. 7(c)) and the core at the end of the acid injection (Sequence R, Fig. 7(d)).

- Contrary to the finding based on 2-D slices that there is almost no expansion of the wormhole after its initiation, three-dimensional image data show that there was some change in the core during acid injection (not as significant as the wormhole initiation).
- Some wormhole growth in a direction perpendicular to the axial flow was also observed during acid injection. The fact that the core plugs in this set (U1V, U2V and U3V) had a higher permeability in the direction perpendicular to the flow may be responsible for flow in vertical direction.

## 4. Results from the low flow rate case using core U2V

### *4.1. CT-scanning sequences and images*

The core plug sample U2V was also characterized using a dual-energy based mineral characterization

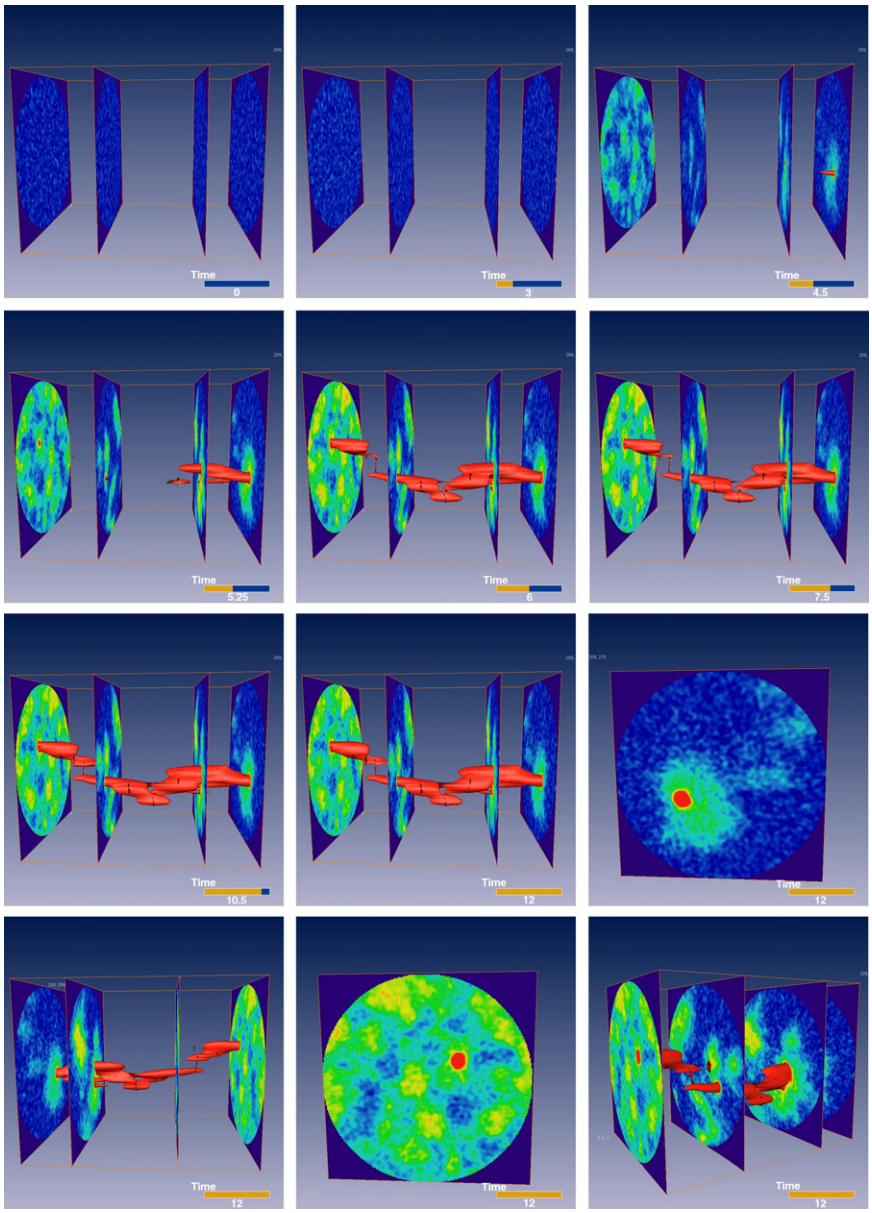


Fig. 8. Snapshots from a three-dimensional movie showing the changes taking place inside the core U2V during acidizing. The core is rotated in the last four snapshots to show the two ends (injection and production).

technique. The dual-energy CT-derived grain density (with the assumption that only calcite and dolomite are present in the core) was found to be 2.74 g/cm$^3$ (higher than the conventional core analysis derived values of 2.69 g/cm$^3$ prior to test and 2.70 g/cm$^3$ after the test). CT-based porosity was calculated using image subtraction technique following saturation of the core with brine. The average porosity of sample U2V using this technique is found to be 10.5 vol.%, compared to conventional core analysis derived value of 9.8 vol.% prior to the test.

A total of 22 sequences of CT image data were collected on the core sample U2V during the test. In each scan sequence the core was scanned at 10 fixed positions (marked from 0 through 9 in the slice images), 5-mm apart from each other. The time taken between two subsequent slices was 8.13 s on the average (includes scan, reconstruction and table movement times) and the average time difference between the first and the tenth slices in a sequence was 80 s. At the flow rate of acid used (0.2 cm$^3$/min) this 80 s time

difference represents a difference of 0.271 $cm^3$ or 0.0457 PVI. The important sequences are shown in Table 3.

Fig. 7(a) shows CT slices immediately after the start of acid injection (Sequence E, 0.04 PVI). The core slices look the same until Sequence I (0.32 PVI, Fig. 7(b)) which shows some changes taking place in the first three slices. By the next sequence (Sequence J, 0.39 PVI), the wormhole path was almost complete (large differences, shown by large circular spots in Fig. 7(c)). By taking the time for acid to reach the third slice in Sequence J, the time of wormhole initiation is 718 s or 0.404 PVI. Acid injection at 0.2 $cm^3$/min was continued until Sequence P (with total injection of 2.02 PVI of acid) when the rate was changed to 1 $cm^3$/min (Sequence Q for another 1.64 PVI) and then to 5 $cm^3$/min (Sequence R, for another 3.47 PVI, Fig. 7(d)). Some minor changes were observed in the slice and slab images based on this increase in the flow rate after wormhole initiation.

Several three-dimensional mpeg movies based on Sequences E through Q during the emulsified acid injection were generated. For the movies three-dimensional data (210×210×10, in FLD format) from all the sequences (E through R) were loaded simultaneously into the program and animations of the isosurface representing the wormhole were created by running through each sequence. Snapshots from one of the movies are shown in Fig. 8. Only four out of the 10 slices are shown to avoid cluttering of the display area. The injection end is on the left and the production end is on the right. The wormhole is shown by an isosurface in the middle of the images. Fig. 9 shows that the higher concentration of calcite may facilitate the initiation of wormhole inside the core.

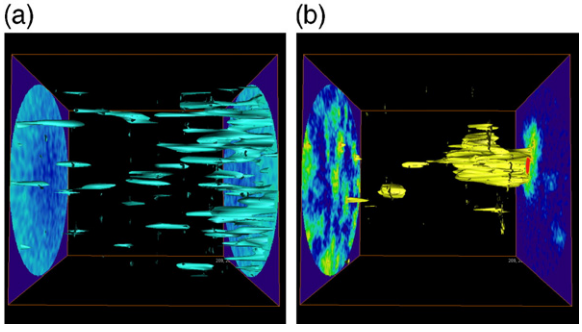


Fig. 9. (a) and (b): Dual-energy derived effective atomic number data showing locations inside the core plug U2V where calcite concentration is the highest (Fig. 9(a)). Image showing the wormhole initiation inside the core plug (Fig. 9(b)).

Table 4
CT-scanning sequences for plug U3V (0.5 $cm^3$/min)

| Sequence name | Description | PVI at the beginning |
|---|---|---|
| B | Scan of saturated core | 0.00 |
| C | First seq. after acid injection started | 0.03 |
| D | Continue acid injection | 0.28 |
| E | Continue acid injection | 0.54 |
| F | Continue acid injection | 0.81 |
| G | Continue acid injection | 1.18 |
| H | Continue acid injection | 1.45 |
| I | Continue acid injection | 1.73 |
| J | Continue acid injection | 2.02 |
| K | Continue acid injection | 2.32 |
| L | Continue acid injection | 5.78 |
| M | End injection at 0.5 $cm^3$/min | 8.22 |

### *4.2. Summary of low flow rate case using core U2V*

This test involving sample U2V, especially with the aid of the three-dimensional movies, allowed several observations to be made on emulsified acid performance. These findings are given below.

- The injection of emulsified acid into brine saturated core was like a miscible process as no piston- or nearly piston-like displacement was observed.
- The initiating of the wormhole with the emulsified acid is an in-situ process rather than a change occurring in the direction of the flow (from inlet to outlet).
- Similar to the test involving U1V, this test (with U2V) the wormhole growth appeared to have initiated at the outlet end of the core (right) rather than at the inlet end. Again, the resolution and the detectability of the CT-scanner may have played a role in this appearance. With the slower injection rate used (0.2 $cm^3$/min) there was a better control over the lag time due to CT-data acquisition and reconstruction (amounted to 81 s between the first and the last slice in this case), the movie confirmed that the wormhole did initiate at the outlet side of the plug. This further confirms the delay in acid reaction caused by injecting the acid in an emulsified form.
- At the slow rate of injection used (0.2 $cm^3$/min, i.e., 0.84 ft/d) no changes could be seen in the first four sequences of scanning. The wormhole was first seen in the CT slices from approximately 0.4 PVI.
- The three-dimensional image data on prolonged injection of acid following wormhole development show some changes in the core taking place although it is not as significant as the wormhole initiation.

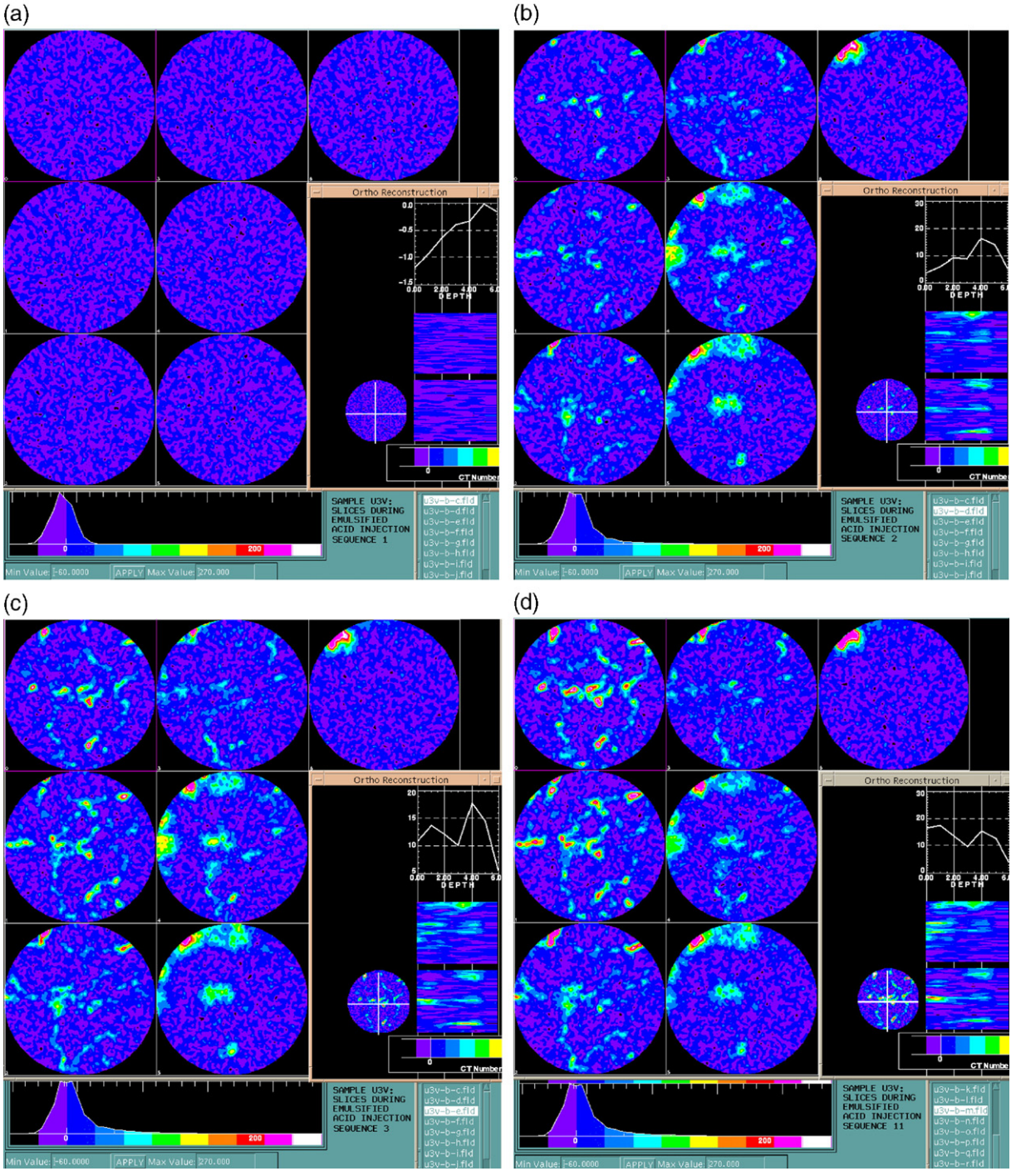


Fig. 10. (a), to (d): Image plates of the core plug U3V right after the acid injection started (Sequence C, Fig. 10(a); the wormhole is seen developing along the top part of the slices in Fig. 10(b) (Sequence D); the wormhole is fully developed in Fig. 10(c), (Sequence E); and slices at the end of acidizing in Fig. 10(d) (Sequence M).

- Increasing the acid injection rate to 1 $cm^3$/min and then to 5 $cm^3$/min following the wormhole development by acid did not result in significant additional wormhole generation for the core plug tested. Some carefully-designed tests using long cores may shed additional light on this issue.

## 5. Results from the medium flow rate case using core U3V

### 5.1. CT-scanning sequences and images

Similar to the two previous samples, Sample U3V was also characterized using a dual-energy based mineral characterization technique. Although taken from almost the same depth as Samples U1V and U2V, Sample U3V is unique in having some embedded stylolites (tooth-like, serrated, interlocking surfaces most commonly seen in carbonates, which are thought to form by pressure solution during diagenesis). One of the goals of doing the test with U3V was to examine the effect of stylolite on acid injection and wormhole generation. The dual-energy CT-derived grain density (with the assumption that only calcite and dolomite are present in the core) was found to be 2.76 g/cm$^3$ (higher than the conventional core analysis derived values of 2.68 g/cm$^3$ prior to test and 2.70 g/cm$^3$ after the test). The porosity calculated using the same technique was also higher, 11.4 vol.%, compared to 8.4 vol.% prior to the test using conventional technique. Porosity due to vacuum saturation was also calculated for Sample U3V (saturation technique) and it was 7.7 vol.% (close to the conventional core analysis derived 8.4 vol.% prior to the test).

A total of 24 sequences of CT image data were collected on the core sample U3V during the test. Table 4 gives the details of the sequences. In each scan sequence the core was scanned at 7 positions (marked from 0 through 6 in the slice images), 5-mm apart from each other. The time taken between two subsequent slices was 8 s on the average (includes scan plus reconstruction times) and the average time difference between the first and the seventh slices in a sequence was 56 s. At the flow rate of acid used (0.5 cm$^3$/min) this represents a difference of 0.467 cm$^3$ or 0.131 PVI.

Fig. 10(a) and (b) show two stages right after the start of acid injection at 0.5 cm$^3$/min (Sequences C and D; 0.03 and 0.28 PVI, respectively). Although Fig. 10(a) (Sequence C) does not show any change, Fig. 10(b) shows some changes in most of the slices. The bright spot seen at the top of several slices starting from the third slice is the wormhole, which developed rather quickly in this test (135 s from acid injection, 1.125 cm$^3$, or 0.315 PVI). Since this top section of the core plug also contains the stylolite, it may be postulated that its presence provided a preferential path for the emulsified acid to create the wormhole. The wormhole was seen in all the slices from Sequence C (0.03 PVI) and the acid injection was continued at the same rate until Sequence M (8.22 PVI). The core was then flushed with brine for post-acidizing permeability measurement.

A three-dimensional mpeg movie based on Sequences C through M during the emulsified acid injection was generated. For the movies three-dimensional data ($220 \times 220 \times 7$) from all the sequences were loaded simultaneously into the three-dimensional visualization program and animations of the isosurface representing the wormhole were created by running through each sequence. Some snapshots from the movie are shown in Fig. 11. Only four out of the seven slices are shown to avoid cluttering of the display area. The injection end is on the left and the production end is on the right. The wormhole is shown by a bright isosurface.

In order to study the influence of porosity on the location of wormholes, the high-porosity streaks within the core based on CT-derived brine saturation data (Fig. 12(a)) are plotted next to the image showing wormhole location inside the core plug (Fig. 12(b)). The images show that higher porosity may have some influence on the wormhole location.

### 5.2. Summary of the medium flow rate case using core U3V

The three-dimensional movies for Sample U3V demonstrated similar observations as those for the other two samples tested – U1V and U2V. Some related observations are listed below.

- Similar to the tests involving U1V and U2V, the wormhole initiation in Sample U3V also appeared to have started at the outlet end of the core (right) rather than at the inlet end. Again, this may be due to the slow release of the acid from the active diesel phase.
- The wormhole initiation was probably facilitated by the presence of stylolite (top section) and also by the presence of higher porosity streaks within Sample U3V. As a result, the wormhole development appeared to be relatively fast.
- The prolonged injection of acid (up to 8.2 PVI), although did not show any appreciable changes in the 2-D slices, did in fact show some changes taking place (additional reaction at the inlet end) long time after the initiation of the wormhole. In the case of the blockage of the primary wormhole, these additional channels may be helpful to production but more detailed economic analysis maybe needed to justify injecting more emulsified acid than necessary.

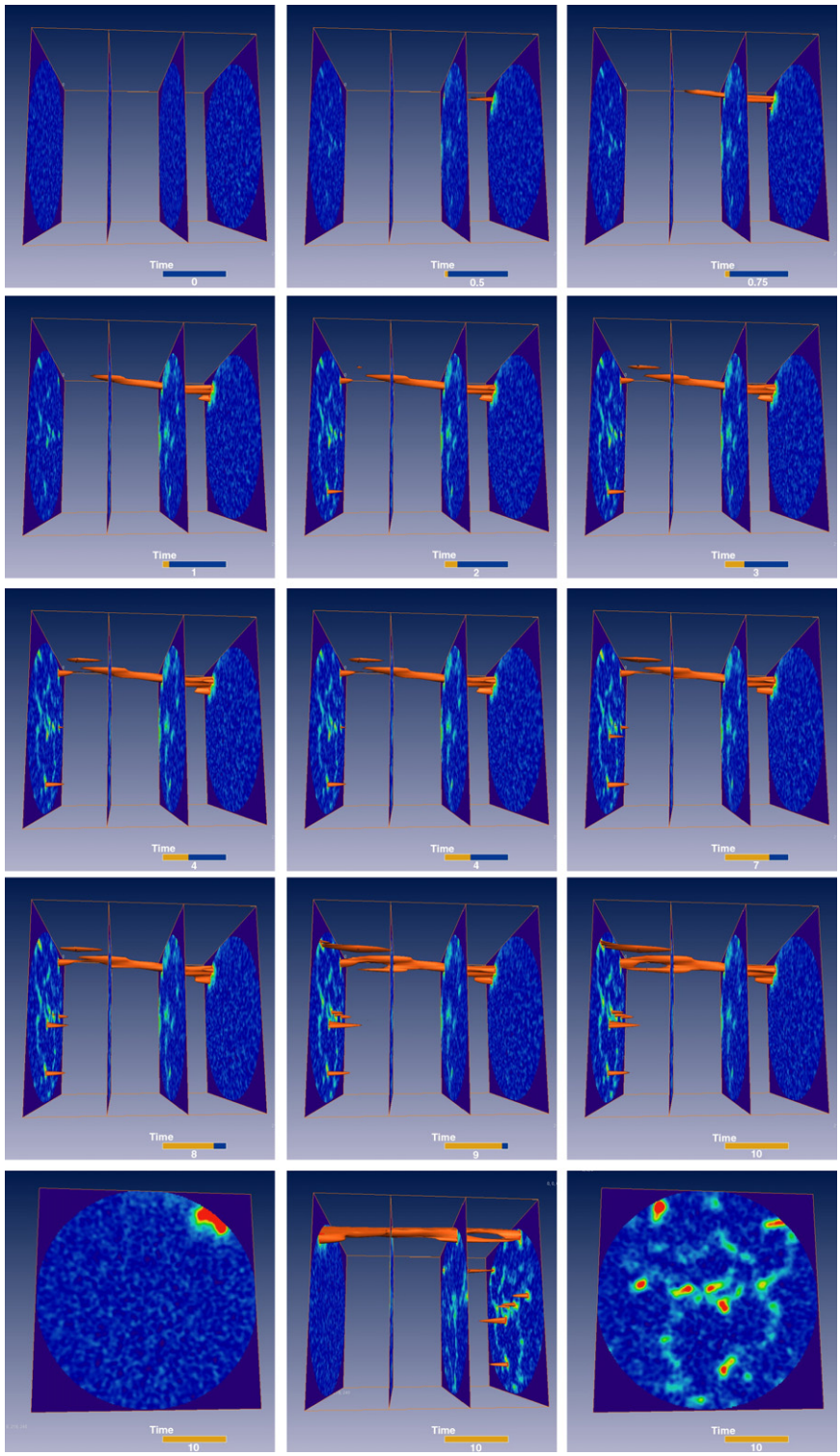


Fig. 11. Snapshots from a three-dimensional movie for the sample U3V showing the changes taking place in the core plug due to acid injection. The core is rotated in the last three snapshots.

## 6. Evaluating acidizing performance based on visual techniques

### 6.1. Wormhole images in dry samples

The samples U1V, U2V and U3V were cleaned with water to remove the acid and the brine and then dried in the oven before scanning them again for the evaluation of the treatment. Fig. 13 shows three isosurface images from the acidized samples U1V, U2V and U3V highlighting the wormholes. The wormhole size is dependent on the value of the isosurface used. All three plugs had almost the same initial permeability and the acid used was the same. The only parameter varied was the flow rate and the samples themselves had different degrees of heterogeneity. In addition, Sample U3V contained stylolites.

The wormhole path in Sample U2V (slowest injection rate) is the most straight and it goes through the middle of the plug. The path in Sample U3V (medium injection rate) is also straight, but it goes through the top section of the sample, possibly aided by the strong stylolite/vug presence in that section. The wormhole path in Sample U1V (fast injection rate) is the most tortuous and broadest (at the same isosurface value). From the limited amount of data available, it appears that a higher injection rate may have a tendency to create more wormhole channels.

It should be noted that the actual size of the wormholes is far smaller than what they look like in these images. The holes at the inlet and outlet faces of all these plugs were found to measure around 1 mm in diameter whereas the images make them appear larger. Fig. 14 shows the photographs of these three samples highlighting the injection and production ends after acidizing. The tip of the wormhole for each plug is shown with an arrow.

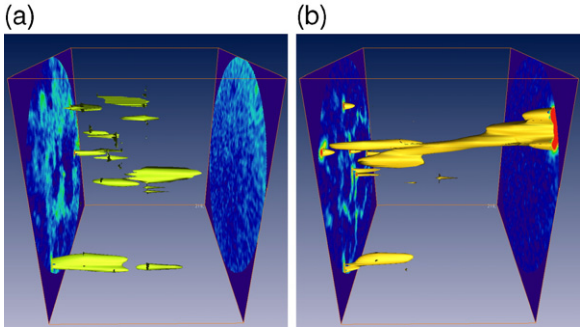


Fig. 12. (a) and (b): CT saturation derived porosity data showing locations inside the core plug U3V where porosity is the highest (Fig. 12(a)). Image showing the wormhole initiation inside the core plug (Fig. 12(b)).

By ignoring the inherent heterogeneities (most likely causing acid in the test with U3V to follow a preferential path) in each of the three samples, the acidizing treatment in Sample U1V appears to be the most effective (larger wormhole and faster growth), followed by U2V. The test involving U2V (slowest injection rate) showed the slowest growth of wormhole and at the same isosurface value it showed the thinnest wormhole out of the three. Since the injection rate was the highest for U1V, followed by U3V and U2V, these observations seem to support injection rate as being one of the most important factors in wormhole development and growth using emulsified acid.

Fig. 15 shows a summary of the effect of the acid injection rate on wormhole initiation time and the corresponding pore volume injected for the three samples U1V, U2V and U3V. Since almost the same amount of time was needed for the wormholes to connect the inlet and outlet of each core, the relationship seen in Fig. 15 is also valid for the effect of wormhole growth rate in these short cores.

### 6.2. Criteria and limitations of visual evaluation techniques

At present permeability measurement (using either the wet core during the test or dry core before and after the test) is the only criterion used for evaluating acidizing performance. However, this type of evaluation does not provide any information on the actual wormhole created or its sustainability. An evaluation technique based on the comparison of isosurfaces at the same value may serve as a yardstick for comparing the emulsified acid performance. Some of the criteria that can be important are:

- Speed of wormhole initiation and growth,
- Shape (tortuous versus straight), and
- Size (broad and multi-channeled versus narrow)

One should be cautioned however, that the generation of wormhole isosurfaces depends heavily on interpolations and other mathematical techniques. Unless the data collected have the right resolution, the evaluations will remain qualitative.

Some of the tests showed very fast wormhole development and for accurate evaluations based on speed, the scanning speed should be much faster than the interstitial (Darcy) velocity. Medical CT-scanners based on the new multi-slice technology usually can provide extremely high speeds of data acquisition. Other features such as spiral scanning, available with newer CT-

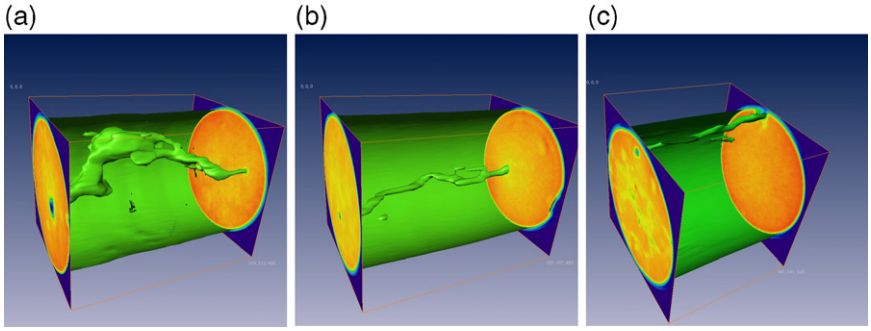


Fig. 13. (a) to (c): Three isosurface plots showing the location of the wormholes within Samples U1V, U2V and U3V, respectively.

scanners should also be useful in out-running the acid injection speed. The time-stamping of slice images by the CT-scanner is generally very helpful in calculating the time of wormhole initiation, which may be used for comparing the performances of different emulsified acids.

## 7. Conclusions

This study examined initiation and propagation of wormholes created by emulsified acid in low permeability reservoir cores. New scanning and data analysis procedures were used to follow the propagation of the acid inside core plugs. The overall findings are summarized below.

1. Real time monitoring using a CT-scanner proved extremely successful in evaluating the performance of emulsified acids in cores. With properly designed tests and relatively fast scanning speeds, CT allows the calculation of the time of wormhole initiation and that of the wormhole connecting the two ends of the core plug.


Fig. 14. (a) and (b): Photographs of the three plugs after acidizing showing the actual wormhole sizes at the two ends (injection end at the top, production end at the bottom).

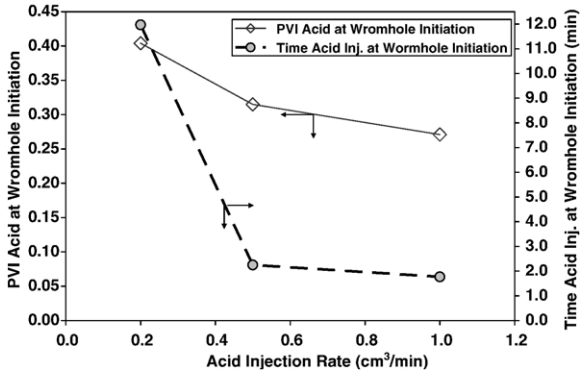


Fig. 15. Effect of injection rate on wormhole initiation time and pore volumes of acid injected.

2. The 2-D CT-slice images generally used have limited capability in monitoring changes taking place inside the core in a dynamic process such as acidizing with emulsified acid. The use of three-dimensional image processing software was necessary for properly evaluating emulsified acid performance inside core plugs. The three-dimensional wormhole image snapshots and movies generated by the advanced image processing software were very useful in observing and evaluating acidizing performance based on visual-based techniques.
3. Based on tests on three very low-permeability core plugs, the wormhole development speed and wormhole size was the highest for the test involving the fastest injection rate. Based on the limited data from these tests, the injection rate appears to be one of the most important factors affecting emulsified acid performance. This finding differs from the observations made by Bazin and Abdulahad (1999) who saw almost a straight line behavior between wormhole breakthrough time and injection rate.
4. Based on the coreflood tests performed in brine-saturated plugs, the propagation of emulsified acid appeared to take place without any immiscible front movement. The wormholes appeared to develop independently as small individual channels which later joined with the others to form a continuous wormhole from one end of the plug to the other.
5. Although the wormholes may have initiated close to the inlet end of the core plugs, the resolution of the CT-scanner used gave the appearance of wormholes initiating at the outlet end of the core rather than at the inlet end as is expected in a typical acid treatment. The role of diesel as a barrier followed by slow release of acid from the emulsion may also have some influence on this appearance.
6. The wormhole initiation may be influenced by the higher concentration of calcite present in the carbonate rock, and the presence of higher-porosity channels and stylolites – all of which provide a preferential path.
7. Although no major changes took place inside the core after acid breakthrough, three-dimensional data on the prolonged acid injection did show some minor changes taking place inside the core plugs, some in the direction perpendicular to flow, which was the path with least resistance (higher-permeability) in those cases.
8. In addition to creating wormholes much faster than the slow injection rate cases, the faster injection rate may also cause additional wormhole channels, which may eventually get connected to result in more sustainable wormhole development.
9. Prolonged injection of acid after wormhole development may help create additional channels, which may have positive effects on oil/gas production, but detailed economic analysis may be needed to justify additional spending for more acid injection.
10. Increasing the injection rate after initial wormhole development apparently did not result in additional wormhole development, but the increasing rate may potentially be beneficial for tests involving long cores. Tests on long cores are also recommended to observe the effects of faster injection rates and the sustainability of wormholes.
11. In addition to the standard evaluation procedure for emulsified acids involving comparison of permeabilities before and after acidizing, the visual evaluation techniques can provide information on the speed of wormhole initiation and growth, shape and size of the wormholes some of which can have long-lasting impacts on oil production.
12. Better evaluation of the performance of emulsified acids using visual techniques can be achieved by higher-resolution and faster CT-scanners, but the progress made so far is a good starting point for future activities.

## Acknowledgments

The authors wish to thank the Saudi Aramco management for the permission to publish this paper.

The authors express their sincere gratitude to their colleagues: Vladimir Velasco, Anwar Hamad, Mohammed Al-Modra, Faisal Al-Dossary, Edwin Caliboso, S. Al-Mutairi, Ali Al-Aamri, O. Al-Fuwaires, and Ali Al-Zahrani.

## References

Akin, S., Kovscek, A.R., 2001. Use of computerized tomography in petroleum engineering research. Annual Report of SUPRI TR 127. Stanford University, Stanford, CA, pp. 63–83.

Al-Anazi, H.A., Nasr-El-Din, H.A., Mohammed, S.K., 1998. Stimulation of tight carbonate reservoirs using acid-in-diesel emulsions – field application. SPE 39418 presented at the SPE International Symposium on Formation Damage Control, Lafayette, LA, USA. February 18–19.

Bartko, K.M., Nasr-El-Din, H.A., Rahim, Z., Al-Muntashri, G.A., 2003. Acid fracturing of a gas carbonate reservoir: the impact of acid type and lithology on fracture half-length and width. SPE 84130 presented at the SPE Annual Technical Conference and Exhibition, Denver, Colorado. 5–8 October.

Bazin, B., Abdulahad, G., 1999. Experimental investigation of some properties of emulsified acid systems for stimulation of carbonate formations. SPE 53237 presented at the SPE Middle East Oil Show held in Bahrain. 20–23 February.

Bazin, B., Bieber, M.T., Roque, C., Bouteca, M., 1995. Improvements in the Characterization of the Acid Wormholing by "In Situ" X-Ray CT Visualizations, SPE 31073 presented at the SPE International Symposium on Formation Damage Control held in Lafayette, Louisiana. February 14–15.

Buijse, M.A., 2000. Understanding wormholing mechanisms can improve acid treatments in carbonate formations. SPEPF 15 (3), 168–175.

Hoefner, M.I., Fogler, H.S., 1985. Effective matrix acidizing in carbonates using microemulsions. Chem. Eng. Prog. 40–44.

Hoefner, M.I., Fogler, H.S., Stenius, H.S., Sjöblom, J., 1987. Role of acid diffusion in matrix acidizing in carbonates. J. Pet. Tech. 203.

Hunt, P.K., Engler, P., Bajsarowicz, C., 1988. Computed tomography as a core analysis tool: applications, instrument evaluation, and image improvement techniques. SPE Formation Evaluation, p. 1203. September.

Kantzas, A., 1990. Investigation of physical properties of porous rocks and fluid flow phenomena in porous media using computer assisted tomography. In Situ 4 (1), 77.

Mohamed, S.K., Nasr-El-Din, H.A., Al-Furaidan, Y.A., 1999. Acid stimulation of power water injectors and saltwater disposal wells in a carbonate reservoir in Saudi Arabia: laboratory testing and field results. SPE 56533 presented at the SPE Annual Technical Meeting, Houston, TX. October 3–6.

Nasr-El-Din, H.A., Al-Anazi, H.A., Mohamed, S.K., 2000. Stimulation of water disposal wells using acid-in-diesel emulsions – field application. SPEPF 15, 176–182.

Navarrete, R.C., Holms, B.A., McConnell, S.B., Linton, D.E., 2000. Laboratory, theoretical and field studies of emulsified acid treatments in high temperature carbonate formations. SPEPF 15 (2), 96–106.

Nierode, D.E., Williams, B.B., 1971. Characteristics of acid reaction in limestone formations. SPEJ 251, 406–418 December.

Siddiqui, S., Funk, J., Khamees, A., 2000. Static and dynamic measurements of reservoir heterogeneities in carbonate reservoirs. SCA paper no. 2000–06 presented at the SCA Symposium held in Abu Dhabi, UAE. October 18– 22.

Siddiqui, S., Grader, A.S., Touati, M., Loermans, A.M., Funk, J.J., 2005. Techniques for Extracting Reliable Density and Porosity Data From Cuttings. SPE 96918 presented at the 2005 SPE Annual Technical Conference and Exhibition held in Dallas, Texas. 9–12 October.

Siddiqui, S., Khamees, A.A., 2004. Dual-energy CT-scanning applications in rock characterization. SPE 90520 presented at the SPE Annual Conference and Exhibition held in Houston, Texas, USA. 26–29 September.

Vinegar, H.J., 1986. X-ray CT and NMR imaging of rocks. JPT, p. 257. March.

Vinegar, H.J., Wellington, S.L., 1987. Tomographic imaging of three-phase flow experiments. Rev. Sci. Instrum. 96 January.

Wellington, S.L., Vinegar, H.J., 1987. X-ray computerized tomography. JPT, p. 885. August.

Williams, B.B., Gidley, J.L., Schechter, R.S., 1979. Acidizing fundamentals. SPE Monograph, vol. 6. Society of Petroleum Engineers, Dallas, Texas, USA. 124 pp.

Withjack, E.M., 1988. Computed tomography for rock-property determination and fluid-flow visualization. SPE Formation Evaluation, p. 696. December.

Withjack, E.M., Devier, C., Michael, G., 2003. The role of X-ray computed tomography in core analysis. SPE paper 83467 presented at the SPE Western Regional/AAPG Pacific Section Joint Meeting held in Long Beach, California. May 19–24.